

LARGE SCALE MARS MAPPING AND ROVER LOCALIZATION USING DESCENT AND ROVER IMAGERY

Rongxing LI*, Fei MA*, Fengliang XU*, Larry MATTHIES**, Clark OLSON**, Yaling XIONG**

* Department of Civil and Environmental Engineering and Geodetic Science, The Ohio State University
470 Hitchcock Hall, 2070 Neil Avenue, Columbus, OH 43210, USA

li.282@osu.edu

** Jet Propulsion Laboratory, California Institute of Technology
Pasadena, California 91109, USA

HYPERLINKHYPERLINK

Working Group IV/2

KEY WORDS: Bundle Adjustment, Rover Localization, Mars Mapping, Descent Imagery, Rover Imagery.

ABSTRACT

The exploration of Mars by landing robotics requires large-scale mapping of the Martian surface and accurate rover localization. The resolution of the orbiter imagery is too low to provide terrain information for the rover to traverse the Martian surface safely. Future MSP (Mars Surveyor Program) exploration missions will extend the rover exploration range from the landing center region to an area of 10kmx10km. This calls for high precision largescale mapping and rover localization with an accuracy of up to 0.1%. This paper presents a method of large-scale mapping and rover localization using descent and rover imagery. A set of descent imagery and rover stereo imagery, collected during a field test at Silver Lake, CA, in May 1999, is integrated into a bundle adjustment system to localize the rover position. It is demonstrated that rover localization with a RMS of 0.14m, 0.08m and 0.34m in the x, y and z direction, respectively, for a distance of up to 500m, and 0.23m, 0.21m and 0.46m within 1.5km can be achieved. This apparently meets the objective of controlling the rover navigation error within 0.1% (1m for 1km).

1 INTRODUCTION

The Mars exploration architecture often consists of an orbiter, lander, and rover. Accurate navigation and localization of the over relative to the lander are needed so that the rover may safely traverse the Martian surface and communicate with the lander as far away as, for example, 10 km from the lander. This calls for high precision, large-scale mapping of the surface and rover localization with an accuracy of up to 0.1% (Matthies, et al. 1997; Li, et al. 2000). The resolution of the orbiter imagery is too low to provide the needed terrain information. The current navigation data, obtained from a heading sensor, an odometer and other sensors with an error of approximately 10% of the distance from the lander is not sufficient for this task. The unique characteristics of the descent imagery that will be available in the future missions motivate the use of orbital data, descent images, and rover images for accurate rover localization (Matthies, et al. 1997).

The Mars Pathfinder has successfully conducted a near-lander rover mission. The rover Sojourner provided powerful close-range tools for microscale rock investigation, soil research and other scientific objectives within an area of about 10m x 10m from the lander. As part of the Mars Surveyor 2001 mission, it is planned that the Marie Curie rover, which is very similar to the Pathfinder Sojourner Rover, will be sent to Mars. In the 2003 and 2005 Mars Missions, the rover FIDO, a prototype of the Mars Sample Return rovers, will carry the integrated Athena Science Payload to Mars. Research was carried out on rover localization using several different methods. Volpe et al. (1995) used a colored cylinder to provide reasonably accurate position and heading information for the rover within a 10 meter range at an accuracy of typically 5° for heading and 5% for distance. Another approach tested maximum likelihood estimation techniques for performing rover self-localization in natural terrain by matching range maps (Olson, et al. 1998). This technique can find the best position in some discretization of the pose space and does not require an initial estimate of the rover position.

This paper discusses large-scale surface mapping and rover localization using descent and rover imagery based on photogrammetric methods. First of all, a set of descent images at different resolutions is used to construct a DEM by determining the descent imagery orientation parameters. The descent images taken from above 5000m to several meters above the ground have a hierarchy of resolutions (from coarse to fine), which match those of the orbital imagery and the ground lander and rover images. This makes descent imagery extremely valuable to scientists for mission planning and to engineers for operating the rover. Specifically, for rover localization, the descent imagery provides an effective way

to enhance the geometry by integrating orbital, descent and lander/rover images to form an image network. Traditional aerial triangulation is performed on pairs or strips of horizontal imagery at nearly the same altitude and with large areas of overlapping. Here, in contrast, we analyze and test bundle adjustment on descent imagery at several different resolutions. Second, the rover image locations and orientations are precisely determined within the network using an extended bundle adjustment. The combined data set of descent and rover images ensures that rover locations farther away from the lander will be determined at an accuracy close to those near the lander.

We present the results of rover localization tests using descent and rover imagery acquired at the field test site at Silver Lake, CA, in May 1999 (Li, et al. 2000). Different adjustment models have been used to localize the rover, in which ground control points, tie points, camera calibration parameters, and various distortion parameters were taken into account. Using the bundle adjustment system we developed, we are able to integrate the descent imagery and rover imagery to achieve a RMS of 0.14m, 0.08m and 0.34m in the x, y and z directions, respectively, for a distance of up to 500m, and 0.23m, 0.21m and 0.46m within 1.5km. The objective of controlling the navigation error within 0.1% (1m for 1km) is apparently met.

2 DATA ACQUISITION AND PREPROCESSING

Descent imaging systems have been successfully used for lunar exploration to provide impressive views of moon. In future Mars exploration missions, the Mars Decent Imager (MARDI), will acquire data during the moments leading up to the touchdown, from the time that the spacecraft's heat shield falls away until the spacecraft reaches the surface (Malin Space Science Systems 2000). MARDI will be able to image the landing site at an interesting set of resolutions over a wide field of view (FOV). MARDI will be a crucial link between the orbiter and lander observations, providing the context for planning the traverses of the rovers that will roam around, looking for interesting geologic features to study. MARDI has a focal length of 7.135mm, a FOV of 73.4deg and an image size 1024X1024 pixels. The first image will be taken at 5000m height. The resolutions vary from 8.65m per pixel to 9mm per pixel.

Radial lens distortion is the dominant distortion in the descent imagery. Suppose r is the distance of a point on the image from the principal point, δr is the radial lens distortion, k_1, k_2, k_3, k_4 are the coefficients of the radial lens distortion, the correction of radial lens distortion is $\delta r = k_1 r + k_2 r^3 + k_3 r^5 + k_4 r^7$. Decentering distortion is another kind of lens distortion that appears in descent imagery. Suppose x, y are coordinates of a point on the image, δx and δy are decentering distortion corrections in the x and y directions, p_1 and p_2 are coefficients of the decentering distortion, the correction for decentering lens distortion in the x direction should be $\delta x = p_1(r^2 + 2xy) + 2p_2xy$, and in the y direction $\delta y = p_2(r^2 + 2y^2) + 2p_1xy$. Since the descent imagery will be taken starting at an altitude of 5000m, the correction for the Martian curvature will be needed. If H is the imaging height, R the Martian radius (3397 km equatorial radius, 3375 polar radius), f the MARDI focal length, and δr_c the correction for Martian curvature, then

$$\delta r_c = \frac{H r^3}{2 R f^2}.$$

EMBEDEMBEEMBEDEMBED

The field test at Silver Lake, CA conducted in 1999 is described in detail in (Li et al., 2000). 15 descent images and several sets of FIDO Navcam imagery at 5m, 500m and 1.5km away from the descent center were acquired. The distortion of the descent imagery is up to 10 pixels. The distortion of the Navcam imagery is about 0.5 pixel to 1 pixel.

3 A PHOTOGRAMMETRIC MODELING FOR HANDLING DESCENT IMAGERY

3.1 Potential of the Descent Imagery

Conventional aerial photogrammetry is used with horizontal images that are usually taken at nearly the same altitude with a regular overlapping area of about 60%. However, the descent images were acquired at a sequence of decreasing altitudes. Landmarks may appear in multiple descent images with different resolutions, the degree of detail decreasing as the image resolution decreases. It is very difficult to find ground features that appear in all the descent images and are appropriate for selection as tie points. Therefore, most tie points chosen are those that appear in a few adjacent images whose resolution differences are not too large. Thus, the resulting tie points link

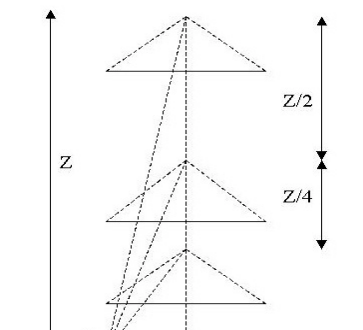


Figure 1. Geometry of descent imaging

the descent image sequence hierarchically in the vertical direction.

In the ideal situation, the descent imagery can be treated as vertical photography (Wolf, 1983), and so the rotation

matrix can be simplified:
$$\begin{pmatrix} m_{11} & m_{12} & m_{13} \\ m_{21} & m_{22} & m_{23} \\ m_{31} & m_{32} & m_{33} \end{pmatrix} = \begin{pmatrix} \cos \kappa & \sin \kappa & 0 \\ -\sin \kappa & \cos \kappa & 0 \\ 0 & 0 & 1 \end{pmatrix}$$
. Based on the collinearity equations:

$x_p = -f \frac{m_{11}(X_p - X_o) + m_{12}(Y_p - Y_o) + m_{13}(Z_p - Z_o)}{m_{31}(X_p - X_o) + m_{32}(Y_p - Y_o) + m_{33}(Z_p - Z_o)}$ and $y_p = -f \frac{m_{21}(X_p - X_o) + m_{22}(Y_p - Y_o) + m_{23}(Z_p - Z_o)}{m_{31}(X_p - X_o) + m_{32}(Y_p - Y_o) + m_{33}(Z_p - Z_o)}$, any two descent images

that share the same feature point can theoretically determine the location of the corresponding 3-D position. Suppose the descent image orientation parameters are fixed, we linearize the collinear equations:

$$v_{x_p} = (f \cos \kappa / (Z_p - Z_o))dX_p + (f \sin \kappa / (Z_p - Z_o))dY_p + (x_p / (Z_p - Z_o))dZ_p$$

$$v_{y_p} = (-f \sin \kappa / (Z_p - Z_o))dX_p + (f \cos \kappa / (Z_p - Z_o))dY_p + (y_p / (Z_p - Z_o))dZ_p$$

From the geometry of vertical photography, we also know that $X_p = (-x_p / f)(Z_p - Z_o)$ and $Y_p = (-y_p / f)(Z_p - Z_o)$. Therefore, the higher the imaging altitude Z_o is, the lower the accuracies of Z_p , X_p and Y_p are. Furthermore, with the increase of imaging altitude, the descent imagery resolution becomes lower, and also the low accuracy of image measurement leads to the lower accuracies of Z_p , X_p and Y_p .

Figure 1 illustrates the geometry of the descent imagery. From any two consecutive descent images, there should be enough tie points to determine the image orientation parameters. With a set of consecutive descent images, a bundle adjustment with enough tie points hierarchically distributed in the vertical direction leads to a high accuracy that is even close to that achievable by horizontal image blocks.

3.2 Least squares adjustment of a free descent image network

In the environment of a Mars landing site, there will be no ground control. The maximum global orientation available may include an approximate lander location, and an azimuth pointing to a landmark defined in the latest global Mars control network with a point accuracy of 750m (Zeitler et al. 2000). So the network computation should be performed as a free network. In our experiment, a local coordinate system is constructed. Because the rover position can be related to the lander, the origin of the local coordinate system should be the lander location. In the bundle adjustment model we apply three constraints: scale, azimuth, and zenith that can be supplied by a landmark relative to the lander. Suppose X_o , Y_o and Z_o are the coordinates of the lander position which will be set to (0,0,0) in the local coordinate system, X_B , Y_B and Z_B are coordinates of a landmark, and D is the distance between them, then the scale constraint is given as $(X_B - X_o)^2 + (Y_B - Y_o)^2 + (Z_B - Z_o)^2 = D^2$. Suppose the azimuth and zenith of the landmark in the local coordinates are β and α , then the zenith constraint and azimuth constraint are represented by

$\tan^{-1}((Z_B - Z_o) / \sqrt{(X_B - X_o)^2 + (Y_B - Y_o)^2}) = \beta$ and $\tan^{-1}((Y_B - Y_o) / (X_B - X_o)) = \alpha$. The network is

solved by an extended least squares adjustment. The measurements of image points with weight P constitute observation equations $V = AX - L, P$ with the constraints represented as $HX = W$. Applying the least squares

principle, $\min(\sum_{i=1}^m v_i^2)$ where v_i are residual of each of the measurements and minimum norm $\min(\sum_{i=1}^n x_i^2)$ where x_i

are unknowns solution, the solution is as follows,

$$X = N^{-1} \left[(A^T P L) + H^T (H N^{-1} H^T)^{-1} (W - H N^{-1} (A^T P L)) \right] \tag{1}$$

$$\sigma_o = \text{sqrt} \left(\min \sum_{i=1}^m r_i^2 \right) / (m - \text{rank}(N)) \tag{2}$$

$$\Sigma_x = \sigma_0^2 \left[N^{-1} - N^{-1} H^T (H N^{-1} H^T)^{-1} H N^{-1} \right] \tag{3}$$

where the normal equation N is decomposed into the full matrices U and V , and the diagonal matrix D as $N = A^T P A = U \cdot D \cdot V^T$, $D = \begin{pmatrix} d_1 & & & 0 \\ & d_2 & & \\ & & \dots & \\ 0 & & & d_n \end{pmatrix}$, and the rank of N is counted as the number of $d_i > 0$, the generalized inverse of N is calculated by $N^{-1} = \left(V \cdot \left[\text{diag} \left(\begin{matrix} 1/d_j \end{matrix} \right) \right] \right) \cdot U^T$.

3.3 Experiment Results

The 10 descent images shown in Figure 2 with imaging heights ranging from 1085m to 8m were selected to conduct a bundle adjustment using the above algorithm. The imaging camera has a focal length of 51.7mm and a field of view of 62°. The image size is 4096X4096 pixels.

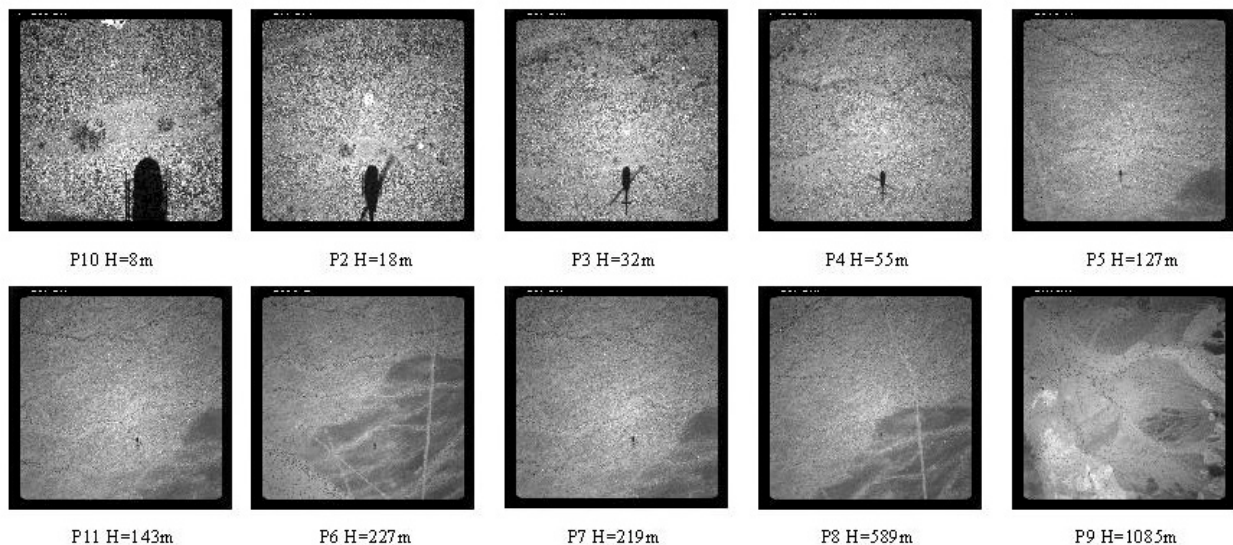


Figure 2. A set of descent images

Within the imaging area, 22 GCPs that have known three dimensional coordinates from the DGPS survey were used as check points. As illustrated in Figure 3, the GCPs are distributed symmetrically around the descent center G1 and the alternative center of G15 in order to evaluate their effect on the accuracy of the network. 72 tie points were manually selected and hierarchically distributed in the vertical direction. A local coordinate system was constructed with the descent center G1 as the origin. In order to formulate the three constraints: scale, azimuth, and zenith, G20 was supplied as a landmark relative to G1. Another 9 GCPs (G2, G3, G4, G5, G6, G7, G8, G9 and G12) which are covered by at least 2 of these 10 descent images were selected as check points.

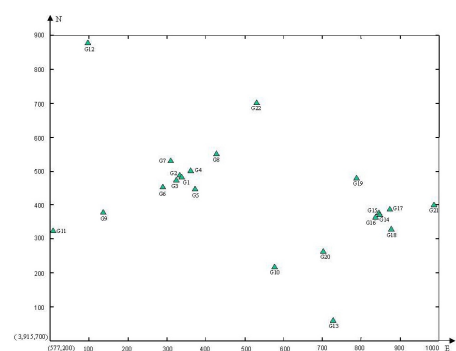


Figure 3. Distribution of ground control points

Table 1 lists estimated standard deviations of the exterior orientation parameters of the descent images. The computational results show that the standard deviations of the exterior orientation parameters of the descending imagery increase as the altitude increases. Comparing this with the results of the bundle adjustment tested on the same 10 descent images but with ground control points (Table 2 of Li, et al. 2000), it can be seen that the standard deviations of the exterior orientation parameters exhibit the same tendency as the imaging altitude increases. The results are nearly the same in terms of accuracy, but the accuracy of the exterior orientation parameters of higher altitude images in the free network is slightly

improved. This demonstrates that the bundle adjustment on descent images without ground control can achieve the same accuracy as that with ground control and the accuracy is more evenly distributed. The comparison also tells us that the accuracy of the exterior orientation parameters of the descending imagery depends on the structure of the network and the distribution of tie points.

Photo-ID	Δ_x (m)	Δ_y (m)	Δ_z (m)	Δ_{ω} (min:sec)	Δ_{ϕ} (min:sec)	Δ_{κ} (min:sec)	Altitude (m)
P1	0.031	0.031	0.036	12:6.4	12:53.7	2:9.8	8
P2	0.058	0.054	0.035	10:28.7	11:13.0	1:42.7	18
P3	0.089	0.086	0.046	9:6.8	9:23.7	1:34.8	32
P4	0.112	0.095	0.053	5:50.8	6:56.0	1:19.3	55
P5	0.214	0.169	0.080	4:30.3	5:50.0	0:58.9	127
P6	0.241	0.194	0.087	4:32.7	5:47.4	1:2.5	143
P7	0.355	0.285	0.116	4:7.7	5:26.3	0:53.4	227
P8	0.356	0.270	0.141	4:14.9	5:29.8	1:1.2	219
P9	0.390	0.506	0.175	2:53.1	2:15.5	0:49.0	589
P10	0.774	0.660	0.336	2:6.6	2:21.6	0:47.3	1085

Table 1. Standard deviations of exterior orientation parameters of the descent imagery

Furthermore, we also analyzed the relationship between errors of the ground point calculated by the adjustment and their distances from the descent center. The RMS errors calculated for 9 checkpoints within 500m from the descent center are 0.24m, 0.15m and 0.38m in the X, Y and Z directions respectively. Figure 4 describes the regression result of this relationship. The curve shows, to some extent, the general trend that the farther away a point is, the lower its accuracy is. But there is no linear relationship between the distance and the point accuracy. In fact, the point accuracy depends on a complex set of factors such as the geometric strength of the network, and the number and distribution of GCPs and tie points, among others. It is clear that Elevation (Z direction) has apparently lower accuracy than the planimetric (X and Y) directions. From this experiment, it is concluded that at least 1 to 3 tie points should be selected in the central and four corner areas of each image.

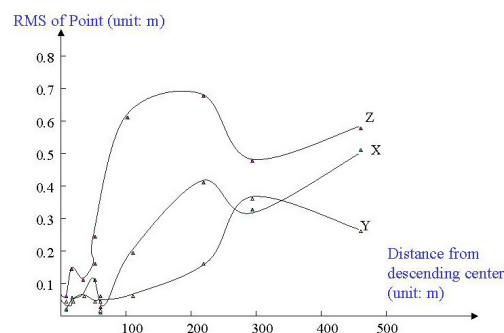


Figure 4. Ground point accuracy vs. distance from the descent center

The RMS calculation results of the bundle adjustment under ground control for 4 check points (G1, G5, G9, and G22) are 0.14m, 0.08m and 0.34m (Li, et al. 2000). Moreover, the diagrams of ground point accuracy vs. distance from the descent center have the same tendency at these different situations.

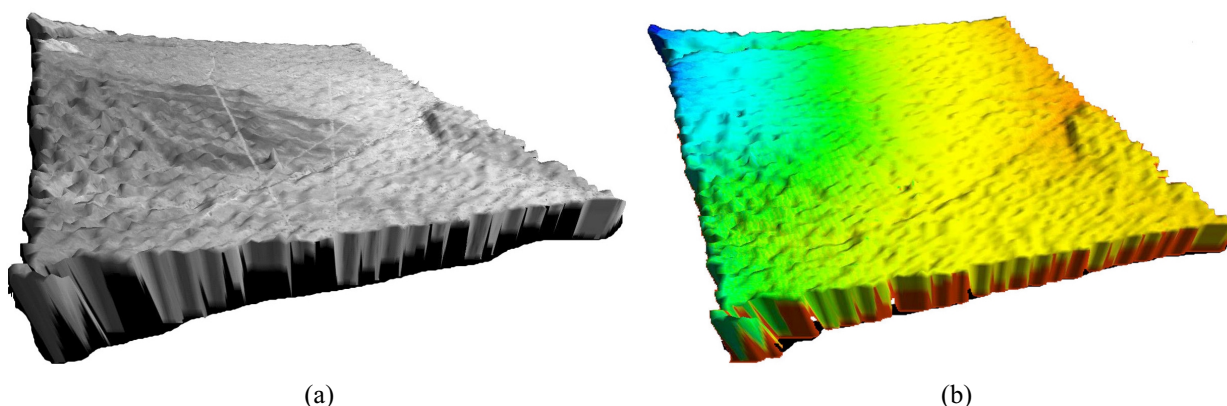


Figure 5. DTM of the Silver Lake test field: (a) DTM draped with a descent image and (b) color coded DTM

The above descent images and the computed orientation parameters were used to generate a digital terrain model (DTM) of the test area at Silver Lake, CA. First, the DTM was filled with an initial elevation computed from a few points, for example, tie points or GCPs. Second, a top-down scheme was used to register 10 pairs of adjacent descent images from high elevations to low elevations. Corresponding features between pairs were then matched through epipolar line searching, area-based correlation, and least squares matching. Third, an initial DTM was built based on the

matched features. Finally, a bottom-up scheme was applied to refine the DTM in which each grid point of the DTM was back-projected onto all possible overlapping descent images to find the corresponding features. A multi-image photogrammetric triangulation provided an improved elevation of the grid point. This process was applied to all the grid points to generate the final refined DTM displayed in Figure 5.

4 ROVER LOCALIZATION USING DESCENT AND ROVER IMAGERY

4.1 Theoretical Aspects of Rover Localization Using Descent and Rover Imagery

With the movement of rover, rover position will be located step by step. The following incremental bundle adjustment is used to locate the rover position. First the observations are decomposed into two parts.

$$v_{m-1} + A_{m-1} X_{m-1} = l_{m-1}, P_{m-1} \tag{4}$$

$$v_m + A_m X_m + B_m Y_m = l_m, P_m \tag{5}$$

where Equation (4) represents the relationship between the observations and unknowns X (including rover position) at step m-1, while Equation (5) represents the next step (m) observations and the previous unknowns X and new unknowns Y. Suppose $N_m^- = \begin{pmatrix} A_{m-1}^T P_{m-1} A_{m-1} + A_m^T P_m A_m & A_m^T P_m B_m \\ B_m^T P_m A_m & B_m^T P_m B_m \end{pmatrix} = \begin{pmatrix} K_m & G_m \\ G_m^T & H_m \end{pmatrix}$, then the solution at step m is determined by

$$\begin{pmatrix} X_m \\ Y_m \end{pmatrix} = \begin{pmatrix} \bar{W}_m (X_{m-1} - F_m (l_m - A_m X_{m-1})) + G_m B_m^T P_m l_m \\ - (B_m^T P_m B_m)^- B_m^T P_m A_m \bar{W}_m (X_{m-1} - F_m (l_m - A_m X_{m-1})) + H_m B_m^T P_m l_m \end{pmatrix} \tag{6}$$

$$\Sigma_m \begin{pmatrix} X_m \\ Y_m \end{pmatrix} = N_m^- N_m N_m^- \tag{7}$$

where $\bar{N}_m^- = (N_{m-1} + A_m^T P_m A_m)^- = (A_{m-1}^T P_{m-1} A_{m-1})^- - F_m A_m (A_{m-1}^T P_{m-1} A_{m-1})^-$, $\bar{W}_m = (I + \bar{N}_m^- A_m^T P_m B_m H_m B_m^T P_m A_m^-)$, $F_m = (A_{m-1}^T P_{m-1} A_{m-1})^- A_m^T (P_m^- + A_m (A_{m-1}^T P_{m-1} A_{m-1})^- A_m^-)^-$.

4.2 Experiment Results and Accuracy Comparison

An experiment to test rover localization using descent and rover imagery was performed with 11 descent images centered around the descent center and 14 pairs of rover images from 5m, 500m and 1.5km away from the lander position (descent center). In order to cover the rover location in the channel area that is about 1.5km away from the descent center, four additional descent images that have flying heights of 300m-800m were also used. The overlap between the images and the two higher altitude descent images is about 30%. Figure 6 shows the footprint of the descent imagery and the rover locations. The resolution difference between the highest descent image (1134m altitude) and the lowest descent image is also significant, for it makes tie point selection difficult. Extensive manual selection and measurement of tie points was required. Figure 7 illustrates the correspondence between descent imagery and rover navigation imagery. Furthermore, to overcome the difficulty with finding correspondences between the descent images and rover images, we utilized the observations of positional and orientation information provided by the rover system as an approximation.

Table 2 lists the standard deviations of exterior orientation parameters of rover images that were taken in three locations marked in Figure 6.

Photo-ID	Δ_X (m)	Δ_Y (m)	Δ_Z (m)	Δ_{ω} (min:sec)	Δ_{ϕ} (min:sec)	Δ_{κ} (min:sec)	Distance to descent center (m)
1356	0.051	0.031	0.038	25:49.3	74:14.6	59:43.3	4.5
1404	0.050	0.032	0.036	24:36.1	73:22.7	57:34.8	4.5
4540	0.316	0.390	0.248	41:7.2	154:19.0	33:37.0	566.0
4611	0.328	0.386	0.253	41:41.4	154:53.0	34:36.0	566.0
1607	0.664	0.533	0.976	17:3.4	113:17.5	16:51.6	1518.3
1617	0.662	0.530	0.978	16:59.2	113:14.3	16:49.9	1518.3

Table 2. Standard deviations of exterior orientation parameters of six rover images

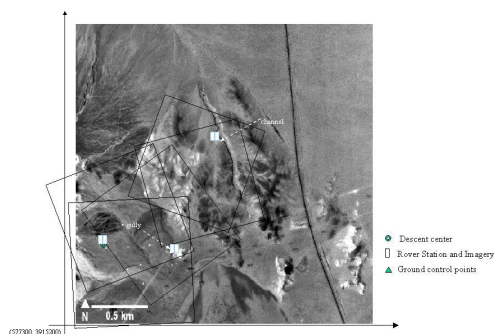


Figure 6. The footprint of descent imagery and rover locations.

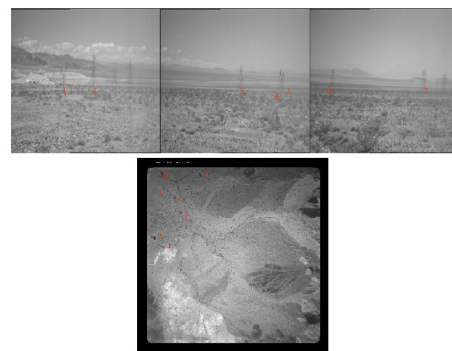


Figure 7. Correspondence between descent imagery (bottom) and rover navigation imagery (top).

The adjustment result shows that the positions of the rover cameras can be localized with an accuracy of 1m within a distance of about 1.5km from the descent center. The computed root mean square errors (RMS) of the ground coordinates of the check points are 0.229m, 0.205m, and 0.455m in the X, Y, and Z directions, respectively. Figure 8 demonstrates the relationship between the point accuracy and the distance from the descent center computed from the free network. In fact, more experiments show that the estimated standard deviation of the unit weight observation of the free network adjustment is better than that of the network with ground control because the entire network is associated with a local coordinate system instead of being forced into a global coordinate system.

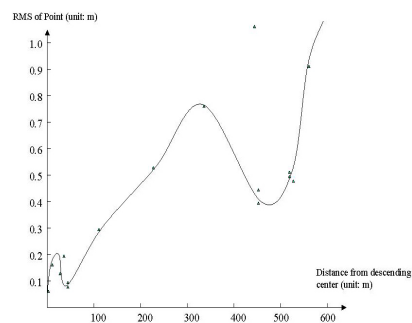


Figure 8. Ground point accuracy vs. distance from the descent center from the adjustment for rover localization

5 CONCLUSIONS

Large-scale mapping of and rover localization on the Martian surface using descent and rover stereo imagery has been studied through the processing of the field data collected at the Silver Lake test site. Based on the above computational results and analysis, the RMS of coordinates in the x, y and z directions are around 0.14m, 0.08m and 0.34m, respectively, for ground points within 500m from the descent center using a network with ground control. They are around 0.23m, 0.21m and 0.46m for ground points within 1.5km from the descent center using a free network adjustment. The rover can be localized at an accuracy of about 1m over a distance of 1.5km. We would like to draw the following conclusions:

- Rover localization through a bundle adjustment using descent and rover stereo imagery has the potential to achieve an accuracy of 0.1% for Mars exploration.
- The result of the free network bundle adjustment demonstrated the geometric and accuracy patterns similar to the bundle adjustment with ground control. This ensures that the developed computational model will fit the Mars landing site environment where no ground control will be available.
- Rover locations at the boundary of the descent image coverage area can also be determined accurately if ground features or landmarks between the rover images and higher altitude images can be recognized and precisely measured.

- One of the keys in successful processing the descent and rover imagery is to select a sufficient number of tie points that are evenly distributed in the imaged area. This is even more crucial to the free network bundle adjustment. High quality tie points between the descent and rover imagery are essential to accurate rover localization using this method.

ACKNOWLEDGMENTS

We wish to thank Dr. C. Toth, Dr. D.G. Brzezinska and Mr. E.Oshel of the Center for Mapping, the Ohio State University for their assistance in field data collection and initial data processing. We also thank Mr. J. Liu and the survey crew of J&P Inc. for the DGPS ground surveying. Data provided by Dr. R. Arvidson of Washington University and JPL/NASA were valuable to the experiment. The project is funded by JPL/NASA.

REFERENCES

- Li, R., F. Ma, F. Xu, L. Matthies, C. Olson and Y. Xiong, Mars Rover Localization Using Descent and Rover Imagery Result of The Field Test at Silver Lake, CA. Proceedings of ASPRS Annual Conference, 2000, Washington D.C.
- Malin Space Science Systems, 2000, http://mars.jpl.nasa.gov/msp98/msss/msss_links/ (20 March 2000)
- Matthies, L., C. Olson, G. Tharp and S. Laubach, 1997. Visual localization methods for Mars rovers using lander, rover, and descent imagery. *International Symposium on Artificial Intelligence, Robotics, and Automation in Space (ISAIRAS)*, pp.413-418, Tokyo, Japan.
- Olson, C. and L. Matthies, 1998. Maximum Likelihood Rover Localization by Matching Range Maps, *Proceedings of the IEEE International Conference on robotics and Automation*, pp.272-277.
- Raeburn, P. and M. Golombek, 1998. *Uncovering the Secrets of the Red Planet: Mars*. National Geographic Society, 231p.
- Volpe, R., T. Litwin and L.H. Matthies, 1995. Mobile Robot Localization by Remote Viewing of a colored Cylinder, Proceedings of the International Conference on Robots and Systems (IROS), Pittsburgh PA, August 5-9 1995.
- Wolf, P., 1983. *Elements of photogrammetry*. McGraw-Hill Publishing Company, 628p.
- Zeitler, W., T. Ohlhof and H. Ebner, 2000. Recomputation of the Global Mars Control Point Network. *Photogrammetric Engineering and Remote Sensing*, 66(2), 155-161.